Investigating Empirical and Theoretical Calculations for Intensity Ratios of L-Shell X-ray transitions in atoms with $39 \leq Z \leq 94$

A. Zidi[1,2], A. Kahoul[1,2*], J.P. Marques[3,4], S.Daoudi[1,2], J.M. Sampaio[3,4], F. Parente[5], A. Hamidani[1,2] S. Croft[6], A.Favalli[7,8], Y. Kasri[9,10], K. Amari[1,2], B. Berkani[1,2]

[1]*Department of Matter Sciences, Faculty of Sciences and Technology, Mohamed El Bachir El Ibrahimi University, Bordj-Bou-Arreridj 34030, Algeria.*
[2]*Laboratory of Materials Physics, Radiation and Nanostructures (LPMRN), Faculty of Sciences and Technology, Mohamed El Bachir El Ibrahimi University, Bordj-Bou-Arreridj 34030, Algeria.*
[3]*LIP – Laboratório de Instrumentação e Física Experimental de Partículas, Av. Prof. Gama Pinto 2, 1649-003 Lisboa, Portugal.*
[4]*Faculdade de Ciências da Universidade de Lisboa, Campo Grande, C8, 1749-016 Lisboa, Portugal.*
[5]*Laboratory of Instrumentation, Biomedical Engineering and Radiation Physics (LIBPhys-UNL), Department of Physics, NOVA School of Science and Technology, NOVA University Lisbon, 2829-516 Caparica, Portugal.*
[6]*School of Engineering, Faculty of Science of Technology, Nuclear Science & Engineering Research Group, Lancaster University, Bailrigg, Lancaster, LA1 4YW, United Kingdom.*
[7]*European Commission, Joint Research Centre, Ispra, I-21027, Italy.*
[8]*Los Alamos National Laboratory, P.O. Box 1663, Los Alamos, NM 87545, USA.*
[9]*Physics Department, Faculty of Sciences, University of Mohamed Boudiaf, 28000 M'sila, Algeria.*
[10]*Theoretical Physics Laboratory, Faculty of Exact Sciences, University of Bejaia, 06000 Bejaia, Algeria.*

[*]Corresponding author. Tel. /Fax (+213) 035862230.
E-mail address: *a.kahoul@univ-bba.dz*

Abstract: The significance of theoretical, experimental, and analytical methods in calculating the intensity ratios of L-shell transitions for diverse elements lies in their widespread applications across various domains, including physical chemistry and medical research. In the present paper, empirical values for intensity ratios were computed through polynomial interpolations using experimental databases within the scope of atomic number $39 \leq Z \leq 92$ for $\frac{I_{L\beta}}{I_{L\alpha}}$ and $\frac{I_{L\gamma}}{I_{L\alpha}}$, and extending to the range of $39 \leq Z \leq 94$ for $\frac{I_{Ll}}{I_{L\alpha}}$. Additionally, new theoretical calculations were conducted using the Multiconfiguration Dirac–Fock Method for specific elements. The obtained results were compared with standard theoretical, experimental, and empirical values, showing a reasonable agreement with them.

Keywords: X-ray fluorescence, intensity ratios, empirical and MCDF calculation

1. Introduction

X-ray fluorescence-based analytical techniques play a crucial role in numerous practical applications across diverse fields, including atomic physics, surface chemical analysis using X-ray fluorescence, medical research, and treatments (such as cancer therapy), and industrial irradiation processing, making intensity ratios essential for these applications (Sahnoun *et al*., 2016). The intensity ratio is an atomic parameter representing the ratio between two transition line intensities. In the context of this paper, attention was given to the intensity ratios within the L shell, specifically $I_{Li}/I_{L\alpha}$ ($i = \beta, \gamma, l$).

L-shell radiative transitions are denoted, following Siegbahn notation, as L_α, L_β, L_γ, and L_l transitions. In Table A, a representation of transitions leading to L lines is provided, alongside the correspondence among Siegbahn, IUPAC, and nL_j electron configuration notations. In this Table, n, l, and j represent, respectively the principal quantum number, the orbital angular momentum, and the total angular momentum quantum numbers. For example, when there is a hole in the L_3 shell and an electron transition from the M_5 shell takes place to fill this hole, it is referred to as the $L_{\alpha 1}$ line.

Multiple efforts have been undertaken to measure and compute L-shell intensity ratios across diverse range elements, employing either a theoretical model or fitting experimental data using empirical formulae. Salem *et al*., (1974) determined the "most probable" values for L X-ray emission rates ($I_{L\alpha 1}$, $I_{L\alpha 2}$, $I_{L\beta 1}$, $I_{L\beta 3}$, $I_{L\beta 4}$, $I_{L\beta 5}$, $I_{L\beta 6}$, $I_{L\beta 2,15}$, $I_{L\gamma 1}$, $I_{L\gamma 2}$, $I_{L\gamma 3}$, $I_{L\gamma 6}$, $I_{L\eta}$, and $I_{Ll}/I_{L\alpha}$) for elements Z=26 to 96 by employing least squares computer fits on experimental data points plotted against atomic number Z. In that same year, Scofield (1974a) conducted a relativistic Hartree–Slater calculation to determine both the total L-shell radiative decay rates and the rates of

emission for individual X-ray lines across elements in the atomic number range $5 \leq Z \leq 104$. Additionally, Scofield (1974b) compiled tabulated values using the same Hartree-Fock model for calculated γ-ray emission rate for a specific set of atoms featuring single vacancies in the L-shell encompassing 21 elements with Z values spanning from 18 to 94. Subsequently, Campbell and Wang (1989) reported a comprehensive collection of L_i (i = 1–3) sub-shell X-ray emission rates for all elements in the range $18 \leq Z \leq 94$, interpolated from the Hartree-Fock model-based values tabulated by Scofield (1974b). X-ray relative intensities of L_i (i = 1–3) subshells for $30 \leq Z \leq 92$, as calculated from the emission rates in Puri's (2007) Dirac-Fock model, have been subjected to least-squares fitting to atomic-number dependent polynomials, these fitted values being intended for incorporation into software packages designed for quantitative elemental analysis using X-ray emission techniques and other related applications. Kumar *et al*., (2010) used the Dirac-Fock model to calculate L intensity ratios for elements with atomic numbers in the range $36 \leq Z \leq 92$. Intensity ratios $I_{Lk}/I_{L\alpha 1}$($k = l, \eta, \alpha_2, \beta_1, \beta_{2,15}, \beta_3, \beta_4, \beta_{5,7}, \beta_6, \beta_{9,10}, \gamma_{1,5}, \gamma_{6,8}, \gamma_{2,3}, \gamma_4$), and $I_{Lj}/I_{L\alpha}$ ($j = \beta, \gamma$) were examined by Puri (2014) for incident photon energies commencing from the binding energy of the L_i sub-shell (i = 1–3), using calculations in the Dirac-Fock model. In the paper of Aylikci *et al*. (2015), interpolations (empirical and semi-empirical) of L-shell X-ray intensity ratios for elements in the range $36 \leq Z \leq 92$.

Recently, our research team presented, in Zidi *et al*. (2024), databases encompassing L-line intensity ratios, including $I_{L\beta}/I_{L\alpha}$, $I_{L\gamma}/I_{L\alpha}$, $I_{Ll}/I_{L\alpha}$, $I_{L\gamma}/I_{L\beta}$, $I_{Ll}/I_{L\gamma}$, $I_{Ll}/I_{L\beta}$, $I_{L\gamma 5}/I_{L\alpha}$, $I_{L\gamma 44'}/I_{L\alpha}$, $I_{L\eta}/I_{L\alpha}$, and $I_{L\gamma 1}/I_{L\alpha}$. This compilation includes experimental values published in 83 research papers spanning the years 1971 to 2023 for elements with atomic numbers $39 \leq Z \leq 94$.

The present study involves determining the empirical values of X-ray emission intensity ratios $I_{L\beta}/I_{L\alpha}$, $I_{L\gamma}/I_{L\alpha}$, and $I_{Ll}/I_{L\alpha}$ by using the experimental data provided in that work, and new theoretical calculations employing the multiconfiguration Dirac-Fock (MCFD) for some elements.

2. Calculation procedure of empirical intensity ratios

The database used in this work relies on our experimental compilation published recently by our group (Zidi *et al*., 2024). We carried out an in-depth analysis of the variations and inconsistencies identified in the experimental ratios presented in Figs.1-3, analyzing these discrepancies with meticulous attention to detail. These differences can be attributed to several factors, including variations in sample preparation, fluctuations in experimental conditions, and potential measurement errors. In particular, the calculation of L-shell intensity ratios is highly sensitive to the preparation of samples, with factors such as surface cleanliness, sample homogeneity, and sample thickness playing pivotal roles. For instance, non-uniform samples can cause differential absorption and scattering X-ray, leading to variability in the measured intensities. Ensuring consistent and precise sample preparation is thus crucial for reliable L-shell intensity measurements. Moreover, experimental conditions such as the stability of the X-ray source, the alignment of detection systems, and the calibration of detectors are crucial in obtaining reliable L-shell intensity ratios. Fluctuations in these conditions can introduce variability into the measurements. For example, instability in the X-ray source can cause variations in intensity, while misaligned detectors may lead to inaccuracies in the detected signal. Calibration errors can introduce systematic biases, further contributing to discrepancies in the measured intensities. The literature suggests that while the outer-shell structure of elements influences their X-ray emission spectra, its impact on L-shell intensity ratios across different compounds is minimal. This implies that discrepancies are likely due to external factors, such as the surrounding matrix and

environmental conditions, rather than the chemical nature of the elements. Matrix effects, where nearby elements alter the apparent intensity of L-shell emissions through mechanisms like absorption or scattering, can notably amplify these differences. Furthermore, local environmental conditions, such as temperature and humidity, can affect the stability and consistency of L-shell intensity calculations. Temperature variations can change the emission characteristics of the sample, and humidity may affect the performance of electronics and detectors, introducing variability into the data. It is important to recognize that the validity and precision of measurements can vary significantly. Measurements performed under highly controlled laboratory conditions including clean rooms with stringent temperature control, are generally more reliable and consistent than those conducted in less controlled environments, which tend to exhibit greater variability. In our study Zidi *et al.*, (2024) we included a table detailing the source, detector, and target sample information for each author, providing a clear and comprehensive overview of the experimental intensity ratios used in this paper. To mitigate variability in our measurements, we utilized a least squares regression method. This approach assigns weights to measurements based on their precision and conditions of acquisition. Measurements obtained under controlled, precise conditions received higher weights, while those with higher variety received lower weights. This approach enhances data accuracy by prioritizing reliable measurements in our analysis, thereby strengthening the robustness and reliability of our study's conclusions.

In this investigation, we computed empirical L-shell intensity ratios, denoted as $I_{Li}/I_{L\alpha}$ ($i = \beta$, γ, and l) by directly interpolating the experimental data. After plotting the experimental values of the intensity ratios as a function of the atomic number Z, shown in Fig.1, Fig.2, and Fig.3, extracted from the databases published by Zidi *et al*. (2024), we propose a second-order polynomial representation for the interpolation of $I_{L\beta}/I_{L\alpha}$ ratio, and a first-order polynomial representation for

$I_{L\gamma}/I_{L\alpha}$ and $I_{Ll}/I_{L\alpha}$ ratios. The empirical $I_{\mathrm{L}\beta}/I_{\mathrm{L}\alpha}$ intensity ratio was calculated for the first time using 678 data points, representing a pioneering utilization of this dataset size. Likewise, the empirical $I_{\mathrm{L}\gamma}/I_{\mathrm{L}\alpha}$ intensity ratio was computed initially with 696 data points, while 585 data points were employed for the inaugural calculation of the empirical $I_{\mathrm{Ll}}/I_{\mathrm{L}\alpha}$ intensity ratio.

- In the intensity ratio $I_{Ll}/I_{L\alpha}$, the experimental values of Aylikci *et al*. (2015) were eliminated due to their dispersion effect in the interpolation.

The polynomial functions utilized for the fitting process are as follows:

$$\left(\frac{I_{L\beta}}{I_{L\alpha}}\right)_{\mathrm{emp}} = \sum_{i=0}^{2} a_i Z^i = f(Z) \tag{1}$$

$$\left(\frac{I_{L\gamma}}{I_{L\alpha}}\right)_{\mathrm{emp}} = \sum_{i=0}^{1} b_i Z^i = g(Z) \tag{2}$$

$$\left(\frac{I_{Ll}}{I_{L\alpha}}\right)_{\mathrm{emp}} = \sum_{i=0}^{1} c_i Z^i = h(Z) \tag{3}$$

The fitted models are represented by solid lines in Figs. 1-3. The fitting coefficients a_i, b_i, and c_i are summarized in Table 1. Furthermore, Tables 2 to 4 present a summary of the empirical calculations of $I_{L\beta}/I_{L\alpha}$, $I_{L\gamma}/I_{L\alpha}$, and $I_{Ll}/I_{L\alpha}$ intensity ratios for elements arranged by their respective atomic numbers.

The total deviation between the calculated empirical $I_{Li}/I_{L\alpha}$ ($i = \beta$, γ, and l) intensity ratios values and the corresponding experimental values are characterized by the root-mean-square error ($\varepsilon_{\mathrm{RMS}}$), which is computed using the following expression (Kahoul *et al*. 2012) :

$$\varepsilon_{RMS} = \left[\sum_{j=1}^{N} \frac{1}{N}\left(\frac{\chi_{j\text{expt}} - \chi_{j\text{calc}}}{\chi_{j\text{calc}}}\right)^2\right]^{\frac{1}{2}} \tag{4}$$

where N represents the total number of experimental data points, χ_{expt} denotes the experimental $I_{Li}/I_{L\alpha}$ ($i = \beta$, γ, and l) intensity ratios, and χ_{calc} signifies the $I_{Li}/I_{L\alpha}$ ($i = \beta$, γ, and l) intensity ratios calculated using the polynomial fits to the respective data sets. The total root-mean-square error (ε_{RMS}) for the empirical results are provided in Table 1 for each ratio.

3. Relativistic calculations

The $I_{Li}/I_{L\alpha}$ ($i = \beta$, γ, and l) intensity ratios are calculated according to the multiconfiguration Dirac-Fock (MCDF) method, implemented by Desclaux (1975) and Indelicato (Indelicato and Desclaux, 1990). The MCDFGME code solves the Dirac-Coulomb-Breit Hamiltonian, incorporating QED corrections through the self-consistent method, and treats some higher-order terms perturbatively. The computation of wave functions adopts a single configuration approach with full relaxation. Due to the time-consuming nature of the calculations, only a restricted set of elements are presented here. The intensity ratios are computed as follows (Hamidani *et al.,* 2023):

$$\left(I_{L\beta}/I_{L\alpha}\right) = \frac{\sum_{i'}\left(2J_{i'}+1\right)\omega_{i'}\left[\sum_{j_3} W^{\mathrm{R}}_{ij_3}(\mathrm{L_2M_4}) + \sum_{j_4} W^{\mathrm{R}}_{ij_4}(\mathrm{L_3N_5}) + \sum_{j_5} W^{\mathrm{R}}_{ij_5}(\mathrm{L_1M_3}) + \sum_{j_6} W^{\mathrm{R}}_{ij_6}(\mathrm{L_1M_2}) + \sum_{j_7} W^{\mathrm{R}}_{ij_7}(\mathrm{L_3O_4}) + \sum_{j_8} W^{\mathrm{R}}_{ij_8}(\mathrm{L_3O_5})\right]}{\sum_i (2J_i+1)\,\omega_i\left[\sum_{j_1} W^{\mathrm{R}}_{ij_1}(\mathrm{L_3M_5}) + \sum_{j_2} W^{\mathrm{R}}_{ij_2}(\mathrm{L_3M_4})\right]}$$

$$+ \frac{\sum_{j_9} W^{\mathrm{R}}_{ij_9}(\mathrm{L_3N_1}) + \sum_{j_{10}} W^{\mathrm{R}}_{ij_{10}}(\mathrm{L_3O_1}) + \sum_{j_{11}} W^{\mathrm{R}}_{ij_{11}}(\mathrm{L_3N_{67}}) + \sum_{j_{12}} W^{\mathrm{R}}_{ij_{12}}(\mathrm{L_1M_5}) + \sum_{j_{13}} W^{\mathrm{R}}_{ij_{13}}(\mathrm{L_1M_4}) + \sum_{j_{14}} W^{\mathrm{R}}_{ij_{14}}(\mathrm{L_3N_4}) + \sum_{j_{15}} W^{\mathrm{R}}_{ij_{15}}(\mathrm{L_2M_3})]}{\sum_i (2J_i+1)\,\omega_i\left[\sum_{j_1} W^{\mathrm{R}}_{ij_1}(\mathrm{L_3M_5}) + \sum_{j_2} W^{\mathrm{R}}_{ij_2}(\mathrm{L_3M_4})\right]} \tag{5}$$

$$\left(I_{L\gamma}/I_{L\alpha}\right) = \frac{\sum_{i'}(2J_{i'}+1)\,\omega_{i'}\left[\sum_{j_3} W^{\mathrm{R}}_{ij_3}(\mathrm{L_2N_4}) + \sum_{j_4} W^{\mathrm{R}}_{ij_4}(\mathrm{L_1N_2}) + \sum_{j_5} W^{\mathrm{R}}_{ij_5}(\mathrm{L_1N_3}) + \sum_{j_6} W^{\mathrm{R}}_{ij_6}(\mathrm{L_1O_3}) + \sum_{j_7} W^{\mathrm{R}}_{ij_7}(\mathrm{L_1O_2})\right]}{\sum_i (2J_i+1)\,\omega_i\left[\sum_{j_1} W^{\mathrm{R}}_{ij_1}(\mathrm{L_3M_5}) + \sum_{j_2} W^{\mathrm{R}}_{ij_2}(\mathrm{L_3M_4})\right]}$$

$$\frac{+\sum_{j_8} W^{\mathrm{R}}_{ij_8}(\mathrm{L_2N_1}) + \sum_{j_9} W^{\mathrm{R}}_{ij_9}(\mathrm{L_2O_4}) + \sum_{j_{10}} W^{\mathrm{R}}_{ij_{10}}(\mathrm{L_2N_{67}})}{\sum_i (2J_i+1)\,\omega_i\left[\sum_{j_1} W^{\mathrm{R}}_{ij_1}(\mathrm{L_3M_5}) + \sum_{j_2} W^{\mathrm{R}}_{ij_2}(\mathrm{L_3M_4})\right]} \tag{6}$$

$$\left(I_{Ll}/I_{L\alpha}\right) = \frac{\sum_{i'}(2J_{i'}+1)\,\omega_{i'}\left[\sum_{j_3} W^{\mathrm{R}}_{ij_3}(\mathrm{L_3M_1})\right]}{\sum_i (2J_i+1)\,\omega_i\left[\sum_{j_1} W^{\mathrm{R}}_{ij_1}(\mathrm{L_3M_5}) + \sum_{j_2} W^{\mathrm{R}}_{ij_2}(\mathrm{L_3M_4})\right]} \tag{7}$$

The expression $W_{ij}^{\mathrm{R}}(\mathrm{L}X)$ denotes the partial radiative transition rate for the emission line LX (where X can be M_1, M_2, M_3, M_4, M_5, N_1, N_2, N_3, N_4, N_5, N_{67}, O_1, O_2, O_3, , O_4, O_5 and L= L_1, L_2, or L_3), while ω_i represents the fluorescence yield of atomic level i within the L-shell one-hole configuration, bearing total angular momentum J_i. Typically, within a given configuration, multiple initial levels exist, and the fluorescence yields within the corresponding equation do not offset each other due to their inclusion in summations. It is necessary to also compute Auger transitions to determine the ω_i values. However, these transitions exhibit minimal variability within each configuration and do not significantly impact the intensity ratios. Thus, to a reasonable approximation, we can cancel out the ω_i in the above equations.

For additional information about the calculation method, readers are directed to Guerra *et al.* (2015) and Guerra *et al.* (2018). The theoretical values are expressed to four significant figures for eight elements ($_{40}$Zr, $_{48}$Cd, $_{50}$Sn, $_{52}$Te, $_{56}$Ba, $_{80}$Hg, $_{83}$Bi, and $_{86}$Rn) in Table 2, 3, and 4 for the intensity ratios $I_{L\beta}/I_{L\alpha}$, $I_{L\gamma}/I_{L\alpha}$, and $I_{Ll}/I_{L\alpha}$, respectively. These tables reveal an exceptional agreement between the empirical results and theoretical calculations using the MCDF method, as will be discussed in Section 4. Notably, the theoretical values show an increase with the atomic number Z.

4. Results and discussion

Tables 2, 3, and 4 present ,respectively, the current calculations of the empirical X-ray intensity ratios $\left(\frac{I_{L\beta}}{I_{L\alpha}}\right)_{\mathrm{emp}}$, $\left(\frac{I_{L\gamma}}{I_{L\alpha}}\right)_{\mathrm{emp}}$, and $\left(\frac{I_{Ll}}{I_{L\alpha}}\right)_{\mathrm{emp}}$ for all elements within the range $39 \leq Z \leq 94$, alongside the theoretical values for elements $_{40}$Zr, $_{48}$Cd, $_{50}$Sn, $_{52}$Te, $_{56}$Ba, $_{80}$Hg, $_{83}$Bi, and $_{86}$Rn, obtained in this work using the MCDFGME code.

In order to effectively compare our empirical and theoretical intensity ratios $I_{Li}/I_{L\alpha}$ ($i = \beta$, γ, and l) results with those from other authors, including experimental, theoretical, and fitted values, the present results $I_{L\beta}/I_{L\alpha}$, $I_{L\gamma}/I_{L\alpha}$, and $I_{Ll}/I_{L\alpha}$ intensity ratios are plotted in Figs.4, 5, 6, respectively, as a function of the atomic number Z. We make the following observations:

- For the empirical values of $\left(\frac{I_{L\beta}}{I_{L\alpha}}\right)_{emp}$ depicted in Fig. 4 and calculated using formula (1), the comparison reveals agreement between our results and those obtained experimentally (Shatendra *et al*. 1983, Raghavaiah *et al*. 1990, Alqadi *et al*. 2023), theoretically (Kumar *et al*. 2010), and via fitting methods (Puri 2014) across all elements with atomic numbers ranging from $_{39}$Y to $_{92}$U. While a slight difference is observed between our empirical and theoretical values and those of Shatendra *et al*., (1983) for elements in the range of $39 \leq Z \leq 64$ and Raghavaiah *et al*. (1990) for the lanthanides, a significant discrepancy is noted between our values and the experimental data of Alqadi *et al*. (2023). In addition, the theoretical values of Kumar *et al*. (2010) and the adjustment values of Puri (2014) are notably distant from our results, except for the heavy elements where there is a good agreement. Moreover, our data exhibit an acceptable range of agreement, with deviations ranging from 0.18 % to 11.63% for Shatendra *et al*. (1983), from 0.82% to 15.38% for Raghavaiah *et al*. (1990) and for Alqadi *et al*. (2023), it spans from 3.41% to 14.81% for most elements. However, a notable variation is observed for some elements, particularly: $_{64}$Gd, $_{65}$Tb, $_{68}$Er, and $_{83}$Bi with deviations of 27.93%, 29.67%, 21.77%, and 25.27%, respectively, for the measurement of Alqadi *et al*. (2023). As we can see in Fig. 1, the values from Puri (2014) for elements in the atomic number range $39 \leq Z \leq 49$ are very different from the current results, the differences ranging from approximately 32.49% to 43.69%. Furthermore, the value for $_{55}$Cs is notably lower, with a relative difference (RD) of 62.26%.

In the range $50 \leq Z \leq 92$, the obtained empirical values are in very good agreement with the fitting values of Puri (2014), with the agreement ranging from 0.21% to 18.39%. For the elements $_{40}$Zr, $_{42}$Mo, $_{44}$Ru, $_{46}$Pd, $_{48}$Cd, $_{49}$In, and $_{50}$Sn, there is a disagreement spanning between 31.46% to 38.97% with the theoretical data of Kumar *et al*. (2010). In this context, the RD is determined by comparing the empirical values obtained to other calculations through the equation,

$$\mathrm{RD}(\%) = \left| \left(\left(\frac{L\beta}{L\alpha} \right)_{\mathrm{exp}} - \left(\frac{L\beta}{L\alpha} \right)_{\mathrm{emp}} \right) \Big/ \left(\frac{L\beta}{L\alpha} \right)_{\mathrm{emp}} \right| \times 100. \quad (8)$$

- The examination of Fig. 5 simplified the process of comparing the theoretical findings of Kumar *et al*. (2010), the empirical data from Puri (2014), as well as the experimental results of Shatendra *et al*. (1983) and Küçükönder *et al.* (2004), with our own empirical calculations of the $\left(\frac{I_{L\gamma}}{I_{L\alpha}} \right)_{\mathrm{emp}}$ intensity ratio computed using the formula (2) across elements with atomic numbers spanning from 39 to 92. The present calculations closely match those reported by Shatendra *et al*. (1983), with RD in the range 0.27%-9.53%, except for $_{47}$Ag (14.59%), $_{49}$In (15.73%), $_{50}$Sn (17.61%), $_{53}$I (25.21%), $_{56}$Ba (19.30%), $_{57}$La (19.66%). Furthermore, it is apparent that our data closely align with the measurements of Küçükönder *et al.* (2004), the agreement being within the range 0.88% to 10.85%, although there are disagreements of 33.43% for $_{72}$Hf, 19.82% for $_{73}$Ta, 19.80% for $_{74}$W, 18.25% for $_{79}$Au, 17.83% for $_{82}$Pb, and 22.94% for $_{84}$Po. We note that our empirical values of $\left(\frac{I_{L\gamma}}{I_{L\alpha}} \right)_{\mathrm{emp}}$ intensity ratio exhibit a disagreement with the theoretical values proposed by Kumar *et al*. (2010), reaching up to 88.96% for elements with Z=39-72. However, for five elements ($_{86}$Rn, $_{88}$Ra, $_{90}$Th, $_{91}$Pa, $_{92}$U), the RD ranges from 4.55% to 12.52%, showing some agreement. Certainly, it is important to highlight that the fitting values from Puri (2014)

consistently fall below our empirical data, with a maximum relative difference (RD) reaching 94.13%. However, these fitting values closely match our theoretical data obtained from the MCDFGME code. Moreover, the results from Puri (2014) and Kumar *et al*. (2010) notably approach our empirical values as the atomic number increases.

- Regarding the $\left(\frac{I_{Ll}}{I_{L\alpha}}\right)$ intensity ratio, Fig. 6 illustrates the progression of our empirical $\left(\frac{I_{Ll}}{I_{L\alpha}}\right)_{emp}$ findings as a function of the atomic number *Z*. This comparison encompasses theoretical values of Scofield (1974a), fitted results from Salem *et al.* (1974), alongside experimental data of Rao *et al.* (1971), Raghavaiah *et al*. (1987), and Ertuğrul (1997). Our current empirical values demonstrate a commendable alignment with the theoretical data suggested by Scofield (1974a), displaying an agreement within the range of 0.53%-11.97% for Z =39-94. When comparing our values to Salem *et al.* (1974) data for the high-Z region ($72 \leq Z \leq 94$), we observe an excellent agreement, with the deviation spanning from 0.54% to 16.06%. In general, the comparison between our empirical results and experimental values reveals a satisfactory agreement. However, significant discrepancies arise for certain elements. For instance, there is a substantial disagreement of 17.75% for $_{65}$Tb in comparison to the values provided by Rao *et al.* (1971). Similarly, there is a deviation between 1.14% to 13.76% for the values reported by Raghavaiah *et al.* (1987). The comparison with Ertuğrul (1997) results fluctuates between 1.53% to 16.12%, except for two elements that show higher disparities (25.13% for $_{90}$Th and 23.40% for $_{92}$U).

5. Conclusion

This study focused on the calculation of empirical intensity ratios of X-ray transitions, including $I_{L\beta}/I_{L\alpha}$, $I_{L\gamma}/I_{L\alpha}$, and $I_{Ll}/I_{L\alpha}$ using an interpolation approach of experimental data

extracted from databases. At the same time, first-principle theoretical calculations were conducted employing the multiconfiguration Dirac-Fock (MCDF) for eight elements. The obtained results show relatively good agreement with those from other research groups, emphasizing the importance of integrating empirical and theoretical approaches to characterize spectroscopic properties of materials in a coherent way over a while dynamic range. The method used to calculate empirical X-ray emission intensity ratios produced reliable values, which can be integrated into formulas and computer codes for calculating X-ray ionization and production cross-sections. However, this research has identified instances where deviations exceeded the expected accuracy of both experimental and theoretical calculations, highlighting the need for further investigation to resolve potential discrepancies. It is crucial to emphasize the critical necessity of acquiring more precise experimental data, particularly for specific values of Z such as 84, 85, 86, 87, 88, 89, and 91, where experimental values are currently lacking. Integrating these experimental benchmarks will not only enhance the reliability and applicability of our findings but also advance our understanding of spectroscopic properties across the periodic table.

6. Acknowledgements

We gratefully acknowledge the support of the DGRSDT, Ministry of Higher Education and Scientific Research, Algeria. This work was done with the support of Mohamed El Bachir El Ibrahimi University, under project (PRFU) N°: B00L02UN340120230004. This work was also supported by the Fundação para a Ciência e Tecnologia (FCT), Portugal through contracts UIDP/50007/2020 (LIP) and UID/FIS/04559/2020 (LIBPhys). S.C. warmly acknowledges the financial support of Lancaster University, and A.F. gratefully acknowledges the support of the Joint Research Centre of the European Commission.

Figure caption:

Fig. 1. Distribution of the experimental $\left(\frac{I_{L\beta}}{I_{L\alpha}}\right)_{EXP}$ values as a function of the atomic number *Z.* The curve is the interpolation according to Eq. (1).

Fig. 2. Distribution of the experimental $\left(\frac{I_{L\gamma}}{I_{L\alpha}}\right)_{EXP}$ values as a function of the atomic number *Z.* The curve is the interpolation according to Eq. (2).

Fig. 3. Distribution of the experimental $\left(\frac{I_{Ll}}{I_{L\alpha}}\right)_{EXP}$ values as a function of the atomic number *Z.* The curve is the interpolation according to Eq. (3).

Fig. 4. The empirical values of the intensity ratio $\left(\frac{I_{L\beta}}{I_{L\alpha}}\right)_{emp}$ and the theoretical values (MCDF) compared to the experimental values from (Shatendra *et al*., 1983, Raghavaiah *et al*., 1990, Alqadi *et al*., 2023), theoretical values of (Kumar *et al*., 2010), and the fitting values of (Puri, 2014) as a function of atomic number *Z.*

Fig. 5. The empirical values of the intensity ratio $\left(\frac{I_{L\gamma}}{I_{L\alpha}}\right)_{emp}$ and the theoretical values (MCDF) compared to the experimental values from (Shatendra *et al*., 1983, Küçükönder *et al.,* 2004, theoretical values of (Kumar *et al*., 2010), and the fitting values of (Puri, 2014) as a function of atomic number *Z.*

Fig. 6. The empirical values of the intensity ratio $\left(\frac{I_{Ll}}{I_{L\alpha}}\right)_{emp}$ and the theoretical values (MCDF) compared to the experimental values from (Rao *et al*., 1983, Ertuğrul, 1997, and Raghavaiah *et al*., 1987) theoretical values of (Scofield, 1974a), and the fitting values of (Salem *et al*., 1974) as a function of atomic number *Z.*

References

Alqadi, M., Al-Humaidi, S., Alkhateeb, H., & Alzoubi, F. (2023). "L-shell x-ray fluorescence relative intensities for elements with $62 \leq Z \leq 83$ at 18 keV and 23 keV by synchrotron radiation". Chin. Phys. B 32(8), 083201.

Aylikci, V., Kahoul, A., Kup Aylikci, N., Tiraşoğlu, E., Karahan, İ. H., Abassi, A., & Dogan, M. (2015). "Empirical and semi-empirical interpolation of L X-ray fluorescence parameters for elements in the atomic range $50 \leq Z \leq 92$". Radiat. Phys. Chem. 106, 99-125.

Campbell, J. L., & Wang, J.-X. (1989). "Interpolated Dirac-Fock values of L-subshell x-ray emission rates including overlap and exchange effects". At. Data Nucl. Data Tables 43(2), 281-291

Desclaux, J. (1975). "A multiconfiguration relativistic Dirac-Fock program". Comput. Phys. Commun. 9(1), 31-45.

Ertuğrul, M. (1997). "Measurement of Ll/Lα intensity ratios for elements in the region $57 \leq Z \leq 92$ by a Si (Li) detector". Spectrochim. Acta Part B: At. Spectrosc. 52(2), 201-204.

Guerra, M., Sampaio, J. M., Madeira, T. I., Parente, F., Indelicato, P., Marques, J. P., Santos, J. P., Hoszowska, J., Dousse, J.-Cl., Loperetti, L., Zeeshan, F., Müller, M., Unterumsberger, R., & Beckhoff, B. (2015). "Theoretical and experimental determination of L -shell decay rates, line widths, and fluorescence yields in Ge". Phys. Rev. A. 92(2), 022507.

Guerra, M., Sampaio, J. M., Parente, F., Indelicato, P., Hönicke, P., Müller, M., Beckhoff, B., Marques, J. P., & Santos, J. P. (2018). "Theoretical and experimental determination of K - and L -shell x-ray relaxation parameters in Ni". Phys. Rev. 97(4), 042501.

Hamidani, A., Daoudi, S., Kahoul, A., Sampaio, J.M., Marques, J.P., Parente, F., Croft, S., Favalli, A., Kup Aylikci, N., Aylikci, V., Kasri, Y., & Meddouh, K. (2023). "Updated database, semi-empirical and theoretical calculation of Kβ⁄Kα intensity ratios for elements ranging from $_{11}$Na to $_{96}$Cm". At. Data Nucl. Data Tables 149, 101549–58.

Indelicato, P., & Desclaux, J. P. (1990). "Multiconfiguration Dirac-Fock calculations of transition energies with QED corrections in three-electron ions". Phys. Rev. A. 42(9), 5139–5149.

Kahoul, A., Aylikci, V., Aylikci, N. K., Cengiz, E., & Apaydın, G. (2012). "Updated database and new empirical values for K-shell fluorescence yields". Radiat. Phys. Chem. 81(7), 713-727.

Küçükönder, A., Durdu, B., Söğüt, Ö., & Büyükkasap, E. (2004). "L X-ray production cross sections, average L shell fluorescence yield and intensity ratios in heavy elements". J. Radioanal. Nucl. Chem. 260, 89-97.

Kumar, A., Chauhan, Y., & Puri, S. (2010). "Incident photon energy and Z dependence of L X-ray relative intensities". At. Data Nucl. Data Tables 96(6), 567-585.

Puri, S. (2007). "Relative intensities for Li (i=1–3) and Mi (i=1–5) subshell X-rays". At. Data Nucl. Data Tables 93(5), 730-741.

Puri, S. (2014). " X-ray relative intensities at incident photon energies across the Li (i=1–3) absorption edges of elements with". At. Data Nucl. Data Tables 100(4), 847-858.

Raghavaiah, C. V., Rao, N. V., Reddy, S. B., Satyanarayana, G., Murty, G. S. K., Rao, M. V. S. C., & Sastry, D. L. (1990). "Lα/Lβ and Lα/Lγ X-ray intensity ratios for elements in the range Z = 55-80". X-Ray Spectrom. 19(1), 23-26.

Rao, P. V., Palms, J. M., & Wood, R. E. (1971). "High- Z L -Subshell X-Ray Emission Rates". Phys. Rev. A. 3(5), 1568-1575.

Sahnoune, Y., Kahoul, A., Kasri, Y., Deghfel, B., Medjadi, D. E., Khalfallah, F., Daoudi, S., Aylikçi, V., Küp Aylikçi, N., & Nekkab, M. (2016). "L_1 , L_2 , and L_3 subshell fluorescence yields : Updated database and new empirical values". Radiat. Phys. Chem. 125, 227-251.

Salem, S. I., Panossian, S. L., & Krause, R. A. (1974). "Experimental K and L relative x-ray emission ratess". At. Data Nucl. Data Tables. 14(2), 91-109.

Scofield, J. H. (1974a). "Relativistic Hartree-Slater values for K and L X-ray emission rates". At. Data Nucl. Data Tables. 14(2), 121-137.

Scofield, J. H. (1974b). "Hartree-Fock values of L x-ray emission rates". Phys. Rev. A, 10(5). 1507-1510.

Shatendra, K., Allawadhi, K. L., & Sood, B. S. (1983). "Energy dependence of photon-induced L-shell X-ray intensity ratios in some high-Z elements". J. Phys. B: Atom. Mol. Phys. 16(23), 4313-4322.

Zidi, A., Kahoul, A., Marques, J.P., Daoudi, S., Sampaio, J.M., Parente, F., Hamidani, A., Croft, S., Favalli, A., Kasri, Y., Amari., K., & Berkani., B. (2024). "Databases of L-shell X-ray intensity ratios for various elements after photon excitation". At. Data Nucl. Data Tables. 157, 101645.

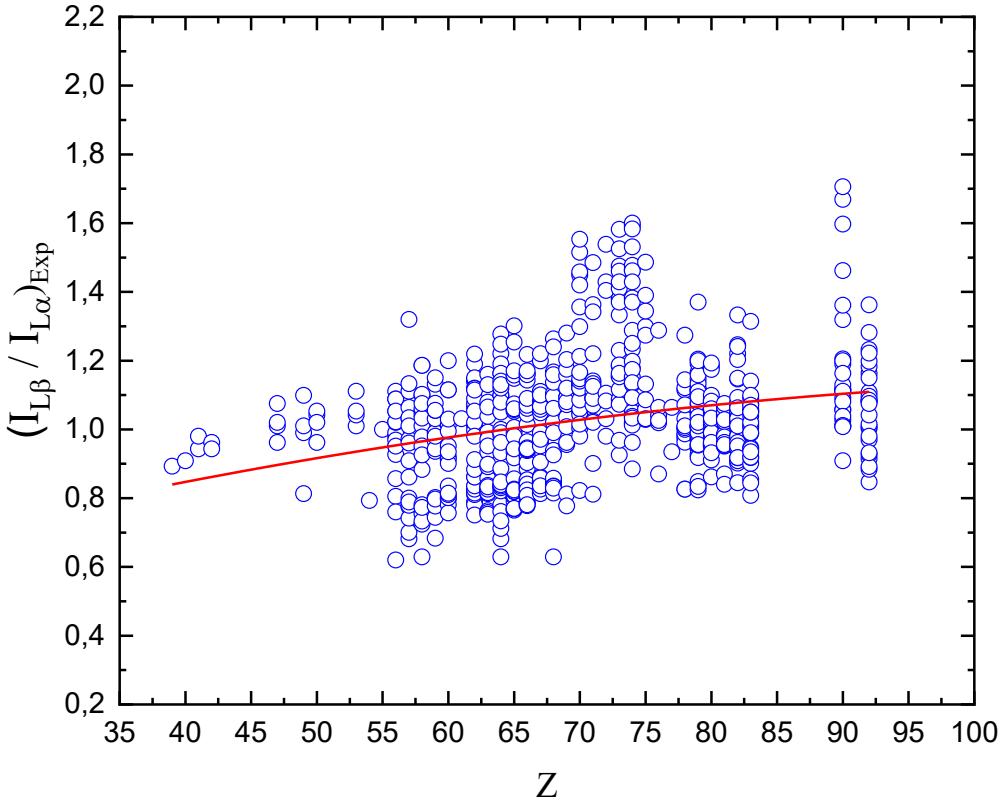
2,2
2,0
1,8
1,6
1,4
1,2
1,0
0,8
0,6
0,4
0,2
$(I_{L\beta} / I_{L\alpha})_{Exp}$
35
40
45
50
55
60
65
70
75
80
85
90
95
100
Z

Figure 1:

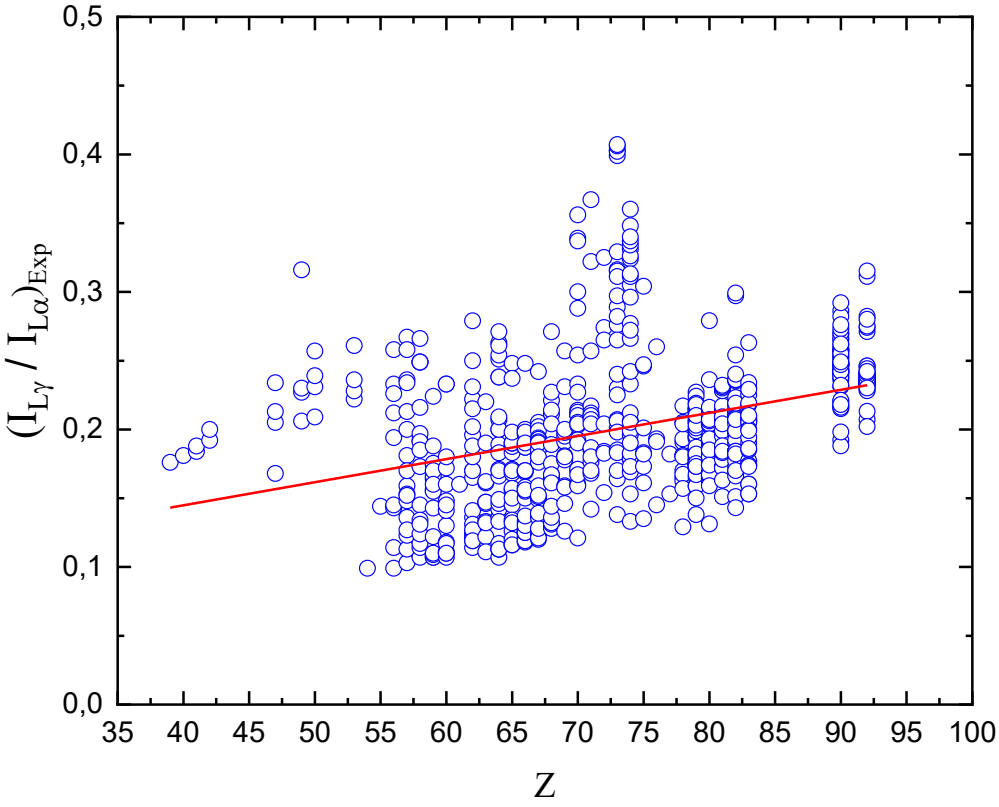
0,5
0,4
0,3
0,2
0,1
0,0
35
40
45
50
55
60
65
70
75
80
85
90
95
100
Z
(I_Lγ / I_Lα)_Exp

Figure 2:

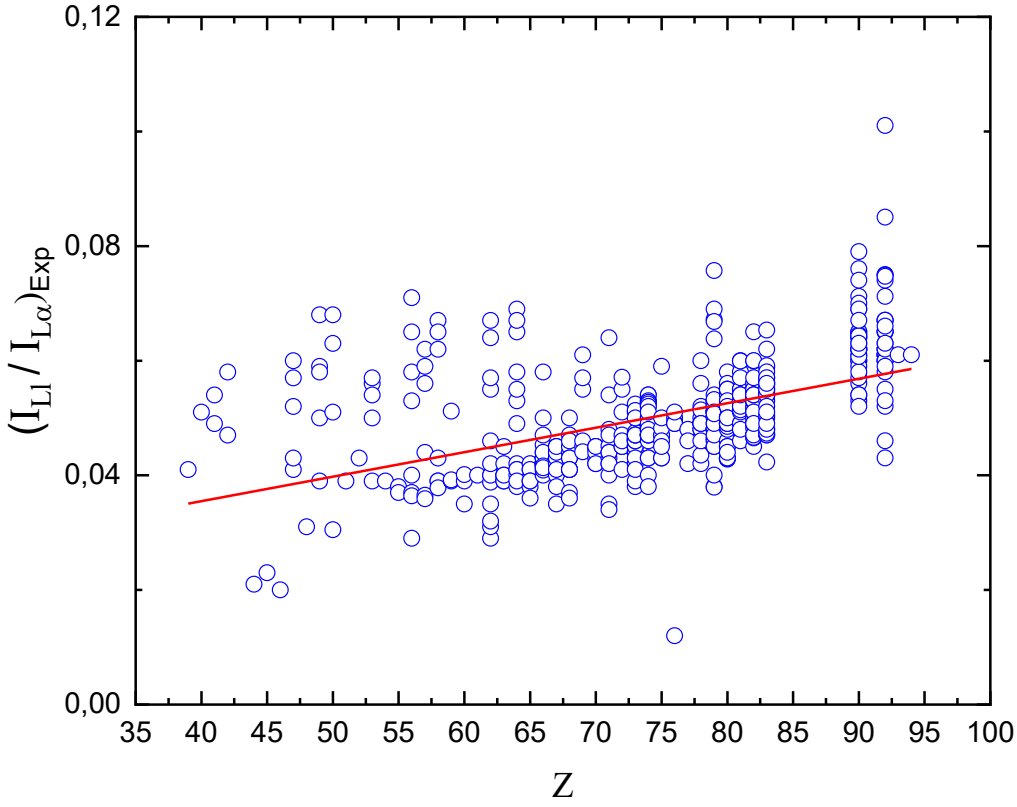
0,12
0,08
0,04
0,00
$(I_{Ll} / I_{L\alpha})_{Exp}$
35
40
45
50
55
60
65
70
75
80
85
90
95
100
Z

Figure 3:

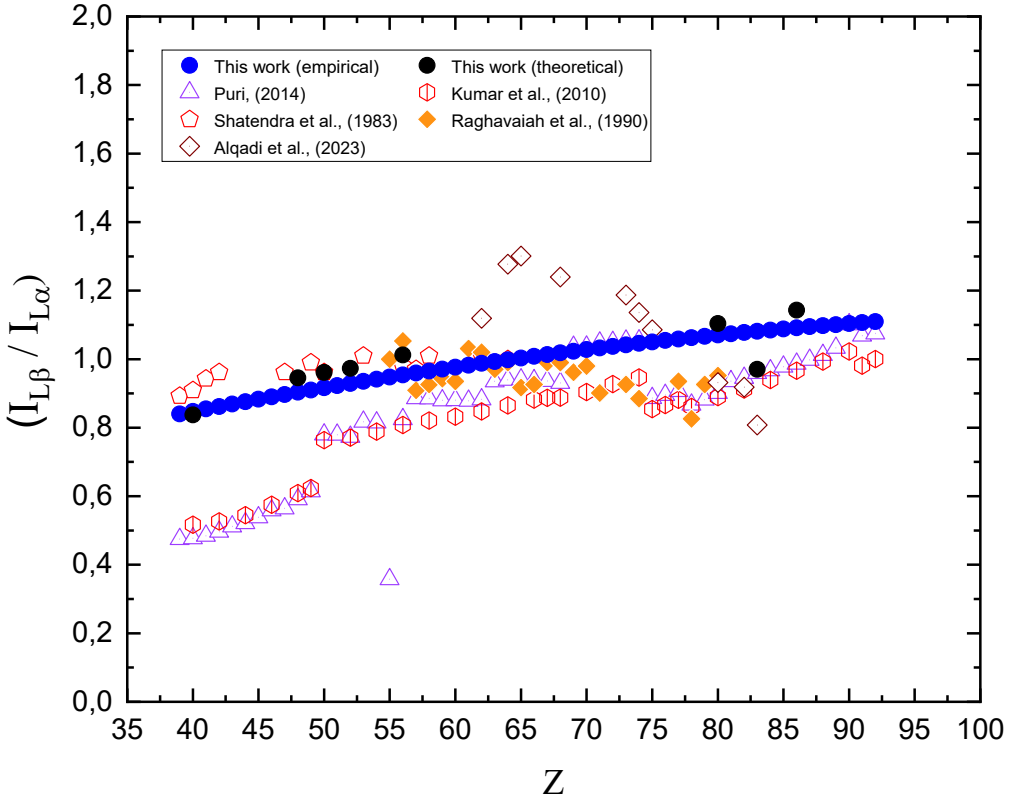
This work (empirical)
This work (theoretical)
Puri, (2014)
Kumar et al., (2010)
Shatendra et al., (1983)
Raghavaiah et al., (1990)
Alqadi et al., (2023)
(I_Lβ / I_Lα)
Z
2,0
1,8
1,6
1,4
1,2
1,0
0,8
0,6
0,4
0,2
0,0
35
40
45
50
55
60
65
70
75
80
85
90
95
100

Figure 4:

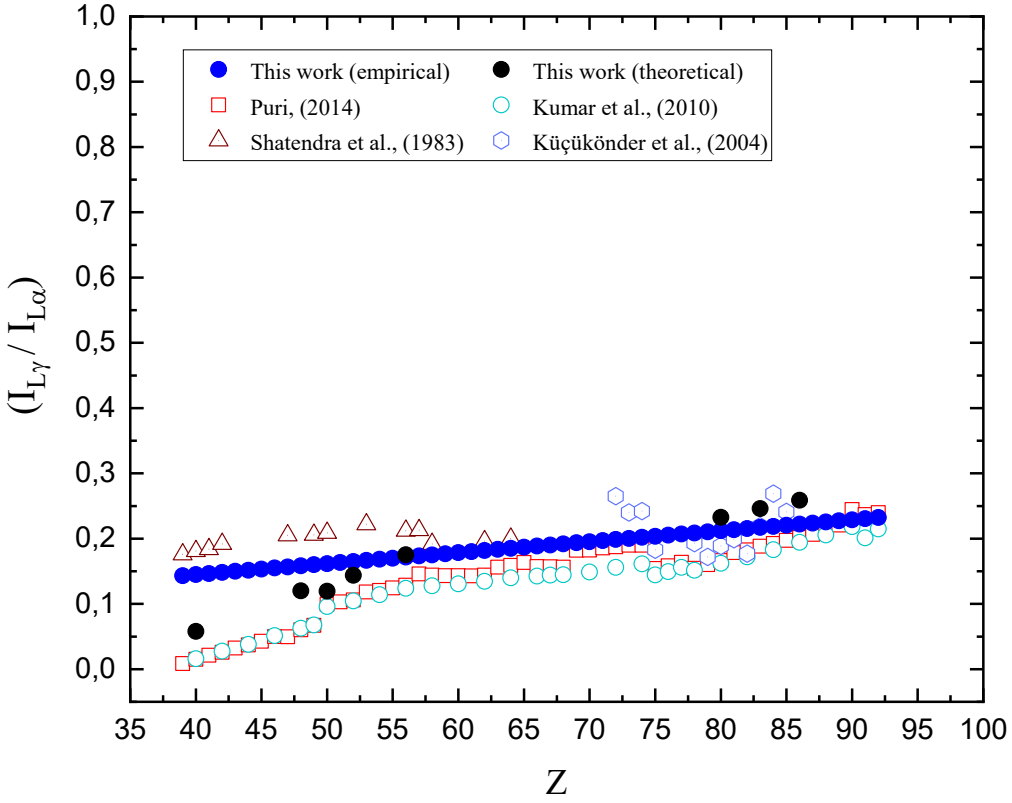
This work (empirical)
This work (theoretical)
Puri, (2014)
Kumar et al., (2010)
Shatendra et al., (1983)
Küçükönder et al., (2004)
(I_Lγ / I_Lα)
Z
1,0
0,9
0,8
0,7
0,6
0,5
0,4
0,3
0,2
0,1
0,0
35
40
45
50
55
60
65
70
75
80
85
90
95
100

Figure 5:

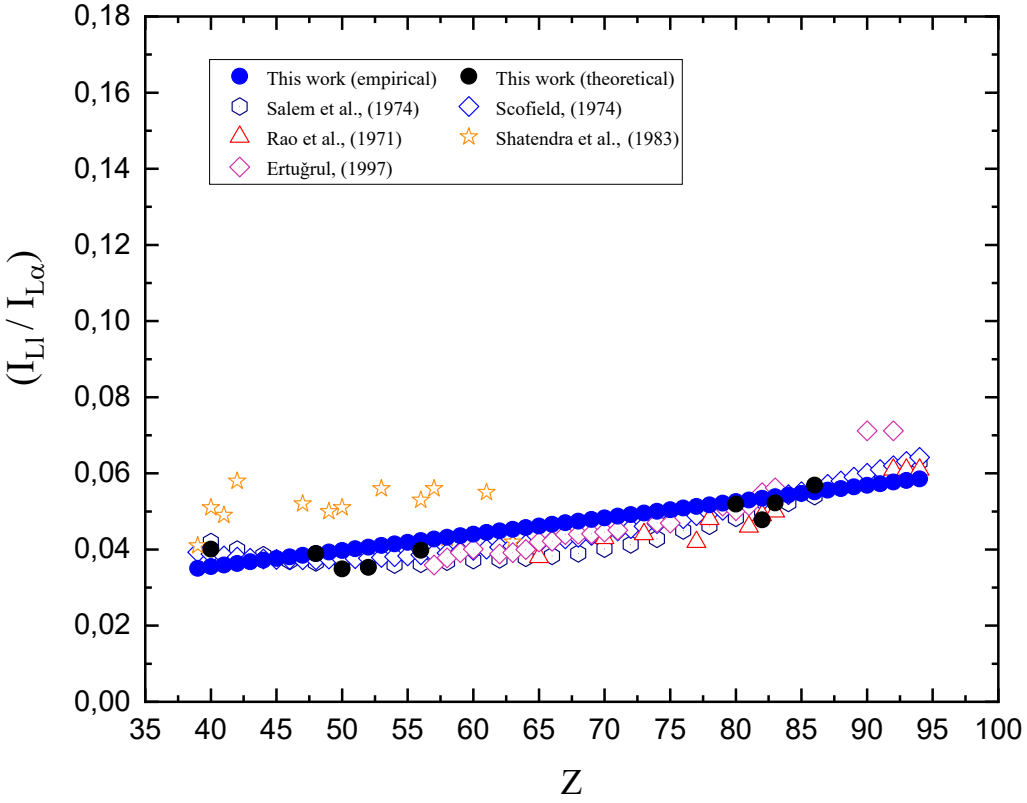
This work (empirical)
This work (theoretical)
Salem et al., (1974)
Scofield, (1974)
Rao et al., (1971)
Shatendra et al., (1983)
Ertuğrul, (1997)
(I_L1 / I_Lα)
Z
0,00
0,02
0,04
0,06
0,08
0,10
0,12
0,14
0,16
0,18
35
40
45
50
55
60
65
70
75
80
85
90
95
100

Figure 6:

Table A. Correspondence between Siegbahn, IUPAC notation diagram lines, and nl_j electron configuration (Ec) notations for radiative transitions.

Siegbahn		IUPAC	EC
L_α	$L_{\alpha 1}$	$L_3 - M_5$	$2p_{3/2} - 3d_{5/2}$
	$L_{\alpha 2}$	$L_3 - M_4$	$2p_{3/2} - 3d_{3/2}$
L_β	$L_{\beta 1}$	$L_2 - M_4$	$2p_{1/2} - 3d_{3/2}$
	$L_{\beta 2}$	$L_3 - N_5$	$2p_{3/2} - 4d_{5/2}$
	$L_{\beta 3}$	$L_1 - M_3$	$2s_{1/2} - 3p_{3/2}$
	$L_{\beta 4}$	$L_1 - M_2$	$2s_{1/2} - 3p_{1/2}$
	$L_{\beta 5}$	$L_3 - O_4$	$2p_{3/2} - 5d_{3/2}$
	$L_{\beta 5}$	$L_3 - O_5$	$2p_{3/2} - 5d_{5/2}$
	$L_{\beta 6}$	$L_3 - N_1$	$2p_{3/2} - 4s_{1/2}$
	$L_{\beta 7}$	$L_3 - O_1$	$2p_{3/2} - 5s_{1/2}$
	$L_{\beta 7'}$	$L_3 - N_{6\,(7)}$	$2p_{3/2} - 4f_{5/2\,(7/2)}$
	$L_{\beta 9}$	$L_1 - M_5$	$2s_{1/2} - 3d_{5/2}$
	$L_{\beta 10}$	$L_1 - M_4$	$2s_{1/2} - 3d_{3/2}$
	$L_{\beta 15}$	$L_3 - N_4$	$2p_{3/2} - 4d_{3/2}$
	$L_{\beta 17}$	$L_2 - M_3$	$2p_{1/2} - 3p_{3/2}$
L_γ	$L_{\gamma 1}$	$L_2 - N_4$	$2p_{1/2} - 4d_{3/2}$
	$L_{\gamma 2}$	$L_1 - N_2$	$2s_{1/2} - 4p_{1/2}$
	$L_{\gamma 3}$	$L_1 - N_3$	$2s_{1/2} - 4p_{3/2}$
	$L_{\gamma 4}$	$L_1 - O_3$	$2s_{1/2} - 5p_{3/2}$
	$L_{\gamma 4'}$	$L_1 - O_2$	$2s_{1/2} - 5p_{1/2}$
	$L_{\gamma 5}$	$L_2 - N_1$	$2p_{1/2} - 4s_{1/2}$
	$L_{\gamma 6}$	$L_2 - O_4$	$2p_{1/2} - 5d_{3/2}$
	$L_{\gamma 8}$	$L_2 - O_1$	$2p_{1/2} - 5s_{1/2}$
	$L_{\gamma 8'}$	$L_2 - N_{6\,(7)}$	$2p_{1/2} - 4f_{5/2\,(7/2)}$
L_l	L_l	$L_3 - M_1$	$2p_{3/2} - 3s_{1/2}$

Table 1. Fitting coefficients according to the formulae (1), (2), and (3).

Intensity ratio	Parameters	Values ± ε	$\varepsilon_{RMS}(\%)$
$\frac{I_{L\beta}}{I_{L\alpha}}$	a_0 a_1 a_2	0.48179312049147 0.01092032342685 -0.00004456088391	16.14
$\frac{I_{L\gamma}}{I_{L\alpha}}$	b_0 b_1	0.07767805617242 0.00167958264881	25.87
$\frac{I_{Ll}}{I_{L\alpha}}$	c_0 c_1	0.01839992102328 0.00042727025389	17.42

Table 2. The empirical $\left(\frac{I_{L\beta}}{I_{L\alpha}}\right)$ intensity ratio and the theoretical calculation using the multiconfiguration Dirac-Fock (MCDF) method for elements with $39 \leq Z \leq 92$.

Z, Element	Empirical calculation	Theoretical calculation (MCDF)
Z=39, Y	0.8399	-
Z=40, Zr	0.8473	0.837
Z=41, Nb	0.8546	-
Z=42, Mo	0.8618	-
Z=43, Tc	0.869	-
Z=44, Ru	0.876	-
Z=45, Rh	0.883	-
Z=46, Pd	0.8898	-
Z=47, Ag	0.8966	-
Z=48, Cd	0.9033	0.9454
Z=49, In	0.9099	-
Z=50, Sn	0.9164	0.9732
Z=51, Sb	0.9228	-
Z=52, Te	0.9292	-
Z=53, I	0.9354	-
Z=54, Xe	0.9416	-
Z=55, Cs	0.9476	-
Z=56, Ba	0.9536	1.0122
Z=57, La	0.9595	-
Z=58, Ce	0.9653	-
Z=59, Pr	0.971	-
Z=60, Nd	0.9766	-
Z=61, Pm	0.9821	-
Z=62, Sm	0.9876	-
Z=63, Eu	0.9929	-
Z=64, Gd	0.9982	-
Z=65, Tb	1.0033	-
Z=66, Dy	1.0084	-
Z=67, Ho	1.0134	-
Z=68, Er	1.0183	-
Z=69,Tm	1.0231	-
Z=70, Yb	1.0279	-
Z=71, Lu	1.0325	-
Z=72, Hf	1.0371	-
Z=73, Ta	1.0415	-
Z=74, W	1.0459	-
Z=75, Re	1.0502	-
Z=76, Os	1.0544	-
Z=77, Ir	1.0585	-
Z=78, Pt	1.0625	-
Z=79, Au	1.0664	-
Z=80, Hg	1.0702	1.1037
Z=81, Tl	1.074	-
Z=82, Pb	1.0776	-
Z=83, Bi	1.0812	0.9701
Z=84, Po	1.0847	-
Z=85, At	1.0881	-
Z=86, Rn	1.0914	1.1430
Z=87, Fr	1.0946	-
Z=88, Ra	1.0977	-

Z=89, Ac	1.1007	-
Z=90, Th	1.1037	-
Z=91, Pa	1.1065	-
Z=92, U	1.1093	-

Table 3. The empirical $\left(\frac{I_{L\gamma}}{I_{L\alpha}}\right)$ intensity ratio and the theoretical calculation using the multiconfiguration Dirac-Fock (MCDF) method for elements with $39 \leq Z \leq 92$.

Z, Element	Empirical calculation	Theoretical calculation (MCDF)
Z=39, Y	0.1432	-
Z=40, Zr	0.1449	0.0579
Z=41, Nb	0.1465	-
Z=42, Mo	0.1482	-
Z=43, Tc	0.1499	-
Z=44, Ru	0.1516	-
Z=45, Rh	0.1533	-
Z=46, Pd	0.1549	-
Z=47, Ag	0.1566	-
Z=48, Cd	0.1583	0.1200
Z=49, In	0.16	-
Z=50, Sn	0.1617	0.1193
Z=51, Sb	0.1633	-
Z=52, Te	0.165	0.1439
Z=53, I	0.1667	-
Z=54, Xe	0.1684	-
Z=55, Cs	0.1701	-
Z=56, Ba	0.1717	0.1752
Z=57, La	0.1734	-
Z=58, Ce	0.1751	-
Z=59, Pr	0.1768	-
Z=60, Nd	0.1785	-
Z=61, Pm	0.1801	-
Z=62, Sm	0.1818	-
Z=63, Eu	0.1835	-
Z=64, Gd	0.1852	-
Z=65, Tb	0.1869	-
Z=66, Dy	0.1885	-
Z=67, Ho	0.1902	-
Z=68, Er	0.1919	-
Z=69,Tm	0.1936	-
Z=70, Yb	0.1952	-
Z=71 ,Lu	0.1969	-
Z=72, Hf	0.1986	-
Z=73, Ta	0.2003	-
Z=74, W	0.202	-
Z=75, Re	0.2036	-
Z=76, Os	0.2053	-
Z=77, Ir	0.207	-
Z=78, Pt	0.2087	-
Z=79, Au	0.2104	-
Z=80, Hg	0.212	0.2325
Z=81, Tl	0.2137	-
Z=82, Pb	0.2154	-
Z=83, Bi	0.2171	0.2460
Z=84, Po	0.2188	-
Z=85, At	0.2204	-

Z=86, Rn	0.2221	0.2587
Z=87, Fr	0.2238	-
Z=88, Ra	0.2255	-
Z=89, Ac	0.2272	-
Z=90, Th	0.2288	-
Z=91, Pa	0.2305	-
Z=92, U	0.2322	-

Table 4. The empirical $\left(\frac{I_{Ll}}{I_{L\alpha}}\right)$ intensity ratio and the theoretical calculation using the multiconfiguration Dirac-Fock (MCDF) method for elements with $39 \leq Z \leq 94$.

Z, Element	Empirical calculation	Theoretical calculation (MCDF)
Z=39, Y	0.0351	-
Z=40, Zr	0.0355	0.0401
Z=41, Nb	0.0359	-
Z=42, Mo	0.0363	-
Z=43, Tc	0.0368	-
Z=44, Ru	0.0372	-
Z=45, Rh	0.0376	-
Z=46, Pd	0.0381	-
Z=47, Ag	0.0385	-
Z=48, Cd	0.0389	0.0389
Z=49, In	0.0393	-
Z=50, Sn	0.0398	0.0349
Z=51, Sb	0.0402	-
Z=52, Te	0.0406	0.0353
Z=53, I	0.041	-
Z=54, Xe	0.0415	-
Z=55, Cs	0.0419	-
Z=56, Ba	0.0423	0.0398
Z=57, La	0.0428	-
Z=58, Ce	0.0432	-
Z=59, Pr	0.0436	-
Z=60, Nd	0.044	-
Z=61, Pm	0.0445	-
Z=62, Sm	0.0449	-
Z=63, Eu	0.0453	-
Z=64, Gd	0.0457	-
Z=65, Tb	0.0462	-
Z=66, Dy	0.0466	-
Z=67, Ho	0.047	-
Z=68, Er	0.0475	-
Z=69,Tm	0.0479	-
Z=70, Yb	0.0483	-
Z=71 ,Lu	0.0487	-
Z=72, Hf	0.0492	-
Z=73, Ta	0.0496	-
Z=74, W	0.05	-
Z=75, Re	0.0504	-
Z=76, Os	0.0509	-
Z=77, Ir	0.0513	-
Z=78, Pt	0.0517	-
Z=79, Au	0.0522	-
Z=80, Hg	0.0526	0.0519
Z=81, Tl	0.053	-
Z=82, Pb	0.0534	0.0478
Z=83, Bi	0.0539	0.0522
Z=84, Po	0.0543	-
Z=85, At	0.0547	-
Z=86, Rn	0.0551	0.0569
Z=87, Fr	0.0556	-
Z=88, Ra	0.056	-

Z=89, Ac	0.0564	-
Z=90, Th	0.0569	-
Z=91, Pa	0.0573	-
Z=92, U	0.0577	-
Z=93, Np	0.0581	-
Z=94, Pu	0.0586	-